Some thoughts on neural network modelling of micro-abrasion-corrosion processes

Srinivasa Pai.P [1], M. T. Mathew [2] , M. M. Stack [3] , L. A. Rocha[2,4],

[1] Dept. of Mechanical Engineering, NMAM Institute of Technology, Nitte, 574110, Karnataka, India.

[2]Research Centre on Interfaces and Surfaces Performance, Azurém, 4800-058 Guimarães, Portugal

[3] Dept. of Mechanical Engineering, University of Strathclyde, James Weir Building, 75 Montrose Street, Glasgow, G1 2XJ, UK

[4]Universidade do Minho, Dept. Eng. Mecânica, Azurém, 4800-058 Guimarães, Portugal

Abstract :

There is increasing interest in the interactions of micro-abrasion, involving small particles of less than 10 um in size, with corrosion. This is because such interactions occur in many environments ranging from the offshore to health care sectors. In particular, micro-abrasion-corrosion can occur in oral processing, where the abrasive component of foods interacting with the acidic environment, can lead to degradation of the surface dentine of teeth.

Artificial neural networks (ANN) are computing mechanisms based on the biological brain. They are very effective in various areas such as modelling, classification and pattern recognition. They have been successfully applied in almost all areas of engineering and many practical industrial applications.

Hence, in this paper an attempt has been made to model the data obtained in microabrasion-corrosion experiments on a steel/ polymer couple and a ceramic/lasercarb

coating using ANN. A Multilayer Perceptron (MLP) neural network is applied and the results obtained from modelling the tribocorrosion processes will be compared with those obtained from a relatively new class of neural networks namely radial basis function (RBF) neural networks.

Keyword: *Tribocorrosion process, Artificial Neural Network (ANN), Multilayer Perceptron (MLP), Radial Basis Function (RBF) neural network*

1.0 Introduction

Tribo-Corrosion involving the interactions of tribological phenomena, such as sliding wear, abrasion or erosion, and chemical phenomena, such as dissolution or passivation, is a complex process and there are many different possible physical interactions, where each of these processes are modified either in a positive or negative direction. Many attempts have been made to investigate the tribocorrosion behaviour of various metallic couples using traditional tribometers, such as the reciprocating sliding tribometer and rotating disk apparatus [2-3]. Although there have been a number of studies carried out on the micro-abrasion performance of materials [4-9], few of these have investigated the individual components of the tribo-corrosion interaction at the contact using electrochemical methods. There have, however, been a number of recent attempts to study the effects of microabrasion on the corrosion rate in a quantitative manner [10-11]. These effects are important to characterize as tribological processes in bio-medical conditions typically occur in corrosion solutions in which the pH and electrochemical potential may vary significantly [12-13]. Understanding the combined effects of the

tribological and corrosion variables is vitally important for optimizing materials selection and tribo-corrosion parameters in such conditions.

Artificial neural networks have been used to model tribological processes and provided promising results [14]. The main functions performed by ANNs were predictions (model) and classifications of the process. Prediction may be used for diagnosis, accelerated life-time testing, on-line control of manufacturing processes that involve wear and prediction of the main properties of the mechanical systems, during the conceptual design stage. Both supervised and unsupervised models were used successfully to model the process.

Hence, the main objective of the current work is to employ neural networks to model the obtained results from the micro-abrasion-corrosion results, an area not tackled to date by ANN modelling approaches. Experimental data have been collected from micro-abrasion-corrosion tests on two couples, involving polymer-steel and a ceramic-lasercarb coating. These data have been used to train and test a MLP neural network, which is a commonly and widely used network architecture. The objective of modelling using a neural network has been to estimate Kac and Ka namely the total micro-abrasion-corrosion rate and the total micro-abrasion rate respectively. These results have been compared with that obtained from another network namely Resource Allocation Network (RAN), a RBF based neural network. Based on the findings, the relative advantages and disadvantages of both modelling approaches are addressed in this paper.

2.0 Data collection and Modelling

2.1 Some aspects on experimental details

Microabrasion tests were performed on a commercially available apparatus, the TE-66, microabrasion tester, Figure 1 (Plint and partners (Phoenix, UK)). Essentially in the microabrasion tester, a 25mm ball is located between two-coaxial shafts, each carried in a support bearing. One shaft was driven by a variable speed DC geared motor. A batch counter was provided to measure and control the number of shaft revolutions. A peristaltic pump head was connected to the other end of the shaft and this was used for providing slurry feed to the contact. The test sample was clamped onto a platform, which was fitted to the pivoted L-shaped arm. This arm was rotated around its pivot until the sample came into contact with the ball. The load was applied by adding dead weights to a cantilever arm. The corrosive slurry was stored in a container that could be agitated by means of a laboratory magnetic stirrer and was delivered to the specimen by an integral peristaltic pump. The slurry (concentration of 0.25 $g.cm^{-3}$) was fed to a position just above the contact point and collected in a waste tray underneath. The arm, which holds the sample, could be moved horizontally in order that several tests on a single sample specimen could be carried out. The sample was then removed from the apparatus and the diameter of the resulting abrasion scars was measured with profile projector. Following the test, the worn samples were examined by optical, scanning electron and atomic force microscopy. The approximate error in the experimental data was estimated to be $\pm$ 20 %.

The wear volume was calculated using the standard technique for measuring the wear scar of spherical geometry [5] i.e. the geometry of the wear scar is assumed to reproduce the spherical geometry of the ball, and the wear volume (V) may then be calculated by measurement of either the crater diameter (b) or its depth (h).

$V \approx \pi b^4 / 64\ R$ For $b << R$ ……(i)

where R is the ball radius.

For estimating the corrosion rate, the sample was connected to the working electrode and a reference electrode was connected by capillary tube in order to make contact with the circuit. A Pt-Ti wire mesh was used as an auxiliary electrode. Potential control for corrosion studies was carried out using a Gill AC electrochemical interface (ACM Instruments, UK). The present study is focused on data modelling; hence, other particulars on the experimental procedure are illustrated in the published work [11]. The micro-abrasion-corrosion data were used from the two couples namely (a) Polymer-steel couple and (b) Ceramic-lasercarb coating couple. More details on the experimental work are given in the Table 1 and 2. The SEM image of the SiC abrasive particles and an optical image of the cross-section of the Lasercarb coating are shown in Figure 2(a) and (b) respectively. Typical SEM images of the worn surfaces are given in Figure 2(c and d).

2.2. Modelling using ANN

Artificial Neural Networks (ANN) are computational systems that simulate the neurons of a biological nervous system. Basically, all ANNs have a similar topological structure [15]. Generally there are three layers – an input layer, which receives information from the external world, a hidden layer, which processes the information and an output layer which presents the output to the external world. The arrangement of neurons in each layer is entirely dependent on the user, which depends on the problem to be modelled and studied. There are two types of networks – Supervised and Unsupervised.

Supervised learning neural networks involve the presentation of both input and corresponding output patterns to the neural network during training. The network learns all the patterns at the end of training and then the network is tested for its performance using patterns that are not used for training. The Multilayer Perceptron (MLP) trained network using a Back-Propagation (BP) algorithm is a widely used network type and is commonly applied to all kinds of industrial as well as research modelling problems [15, 16]. Radial Basis Function (RBF) neural networks are a new class of robust neural network that has been used to a limited extent in modelling various research problems. Algorithms based on this type of network has been used to build neural network architecture dynamically during learning and one such network type is the Resource Allocation Network (RAN), which builds its own architecture during training.

2.2.1 Multilayer Perceptron (MLP)

MLP have been applied successfully to solve some difficult and diverse problems by training them in a supervised manner with a popular algorithm known as Back-Propagation (BP) algorithm. [17]. This algorithm allows experiential acquisition of input / output mapping knowledge within the networks. There are basically two passes through the different layers of the network: a forward pass, in which an input pattern is submitted and propagated through the network layer by layer and an output is produced as the actual response of the network. During the forward pass, the synaptic weights are all fixed and in the backward pass, the synaptic weights are adjusted depending upon the error between the actual output and the desired output [17].

Figure 3 shows the architecture of the network. There are three layers – an input, hidden and an output layer. The input layer contains two neurons corresponding to

potential and load for one network and pH and load for another network. The number of neurons in the hidden layer is fixed based on the desired performance from the network. There are two output neurons corresponding to Kac and Ka. The hidden neurons and output neurons have a sigmoidal nonlinearity defined by the logistic function:

$$y_j = 1 / (1 + \exp(-v_j)) \qquad \text{(ii)}$$

where $v_j = \Sigma\, w_{ji}\, \xi_i$ is the net internal activity of neuron j, w_{ji} are the weights between neuron j in the hidden layer and neuron i in the input layer and ξ_i is the input. y_j is the output of the neuron. The training of the network involves propagating all the input patterns through the network layer by layer (called an 'epoch') and then in the backward pass modifying the weights based on the cumulative error computed over the entire training set. The modification of the weights is done as follows:

$$w^{new}_{ji} = w^{old}_{ji} + \Delta w_{ji}, \qquad \text{(iii)}$$

where $\Delta w_{ji} = \eta\alpha\ \Sigma\, \delta_j\, v_j$ and where δ_j is determined by partial differentiation of the total mean square error with respect to the weights. This is performed on the weights between input and hidden and hidden and output layers. η is the learning rate, which controls the effectiveness and convergence of the algorithm and α is the momentum term, which is generally used to accelerate the convergence of the error BP algorithm.

2.2.2. Data set

There are two data sets. The first set consists of data corresponding to weight change for the microabrasion-corrosion interaction of mild polymer/steel couple at various potentials (a) –0.6 V (b) –0.4 V (c) –0.2 V (d) 0 V (e) +0.2 V (refer table 3). The training data consisted of 20 patterns and the test data 5 patterns. The second data set consisted of data corresponding to weight change for the micro-abrasion-corrosion

interaction of Ceramic-Ni-Cr/WC – Lasercarb coating, at fixed potential –0.2 V and various pHs (refer Table 4). The training data consisted of 16 patterns and the test data 4 patterns. The data has been normalized using the method

$$x_{normalized} = x / x_{max} \quad \text{(iv)}$$

were x is the input pattern and x_{max} is the maximum value of the pattern.

The number of neurons in the hidden layer has been varied followed by the values of η and α for desirable performance in terms of minimum training time and error reached. The optimum values for η and α are 0.8. The number of hidden neurons for optimum performance was found to be 15. The network converged to an error of 0.01 in 150,000 epochs.

Similarly the MLP network was trained for the second data set and the values of the parameters for optimum performance were as follows – hidden neurons – 12, $\eta = 0.95$ and $\alpha = 0.05$. The network converged to an error of 0.03 in 125,000 epochs.

2.2.3 Resource Allocation Network

Resource Allocation Network (RAN) is a sequential learning Gaussian Radial Basis Function network. Platt's (1991) [13] motivation for RAN stemmed from the fact that learning with a fixed–size network is a NP-complete problem and by allocating new resources, learning could be achieved in polynomial time. The network learns by allocating new hidden neurons and adjusting the parameters of the existing neurons. If the network performs poorly on a presented pattern, then a new neuron is allocated which corrects the response to the presented pattern. Conversely, if the network performs well on a presented pattern, then the network

parameters are updated using standard a Least Mean Square (LMS) gradient descent. The structure of RAN is the same as that of RBF networks. Each hidden neuron in the network has two parameters called a center x_j and width σ_j associated with it. The activation function of the hidden neurons is radially symmetric in the input space and the output of each hidden unit depends only on the radial distance between the input vector ξ_i and the center parameter x_j for that hidden neuron. The response of each hidden unit is scaled by its connecting weights w_{kj} to the output units and then summed to produce the overall network output. The overall network output is

$O_k = \Sigma_j w_{kj} v, \quad (v)$

where j=1 to c are the number of hidden neurons and $v_j = e^{-\|x_j - \xi_i\| / 2\sigma}$, where v_j is the response of the j^{th} hidden unit, w_{kj} is the weight connecting hidden neuron j to output neuron k, x_j and σ_j are the center and width of the j^{th} hidden neuron respectively.

The learning phase involves allocation of new hidden neurons as well as adaptation of network parameters. The network begins with no hidden neurons. As input-output data are received during training, some of them are used for generating new hidden units. The decision as to whether an input – output pair (ξ_i, ζ_k) should give rise to a new hidden neuron depends on the novelty in the data which is decided using the following two conditions: (i) $d = \| x_j - \xi_i \| > \delta$, (ii) $e = \| \zeta_k - O_k \| > e_{min}$, where δ and e_{min} are thresholds to be selected appropriately. If the above two conditions are satisfied, then the data is deemed to have novelty and a 'new hidden neuron' is added. The first condition says that the input must be far away from all the centers and the second

condition says that the error between the network output and target output must be significant. e_{min} represents the desired approximation accuracy of the network output and the distance δ represents the scale of resolution in the input space [18].

The algorithm begins with $\delta = \delta_{max}$, where δ_{max} is chosen as the largest scale of interest in the input space, typically the entire input space of non zero probability. The distance δ is decayed exponentially $\delta = \max (\delta_{max} e^{(-t/\tau)}, \delta_{min})$. The value of δ is decayed until it reaches $\delta_{min,}$ which is the smallest length scale of interest. This exponential decaying of the distance criterion allows fewer basis functions with large widths initially and with increasing number of observations, more basis functions with smaller widths are allocated to fine tune the approximation. The parameters associated with the new hidden neurons are as follows : $w^{new}_{kj} = e$, $x^{new}_{j} = x_j$ and $\sigma^{new}j = \kappa \|x_j - \xi_i\|$ where κ is an overlap factor that determines the amount of overlap of the responses of the hidden units in the input space. As κ grows larger, the responses of the neurons overlap more and more. When an input-output pair does not pass the novelty criteria, a hidden neuron is not added but the network parameters x_j and w_{kj} are adapted to fit the observation. The width parameter is not adapted [18]. Figure 4 shows the RAN architecture. The data sets used above have been used to train and test RAN.

3.0 Results and Discussion

3.1 Estimation of weight change data

The weight change data may be explained by defining the following terms, using the methodology developed by Yue and Shi [19] in wear analysis and the estimation of weight changes during micro-abrasion-corrosion in previous work [11].

If: $Kac = Ka + Kc$ (vi)

where, Kac is the total microabrasion-corrosion, Ka is the total microabrasion rate, and Kc is the total corrosion rate.

Ka can be written as Kao + Δ Ka, i.e.:

$$Ka = Kao + \Delta Ka \qquad \text{(vii)}$$

where Kao is the microabrasion rate in the absence of corrosion, Δ Ka is the effect of corrosion on the microabrasion.

Kc can be explained as Kco + ΔKc, i.e:

$$Kc = Kco + \Delta Kc \qquad \text{(viii)}$$

where Kco is the corrosion rate in the absence of wear, ΔKc is the effect of microabrasion on the corrosion, or the enhancement of corrosion due to the microabrasion process.

Hence, the total microabrasion – corrosion rate can be given as follows:

$$Kac = Kao + \Delta Ka + Kco + \Delta Kc \qquad \text{(ix)}$$

The results of the various contributions to weight change are given in Table 1. The corrosion rate data, Kc, were derived using Faraday's law, e.g.

$$Kc = Q.(nF)^{-1} \qquad \text{(x)}$$

$$Kc = MIt(nF)^{-1} \qquad \text{(xi)}$$

where Q is the charge passed, F is Faraday's constant (96500 C mol^{-1}), n is the number of electrons involved in corrosion process, I, the total current, t the exposure time and M is the atomic mass of the material. The weight loss due to wear in the absence of corrosion, Kao, was estimated by measuring the weight change in cathodic conditions i.e. at –0.96 V.

3.2 MLP modelling results

MLP has been used to model the microabrasion-corrosion process of steel/ polymer couple and a ceramic/lasercarb coating. The basic objective of modelling is to estimate Kac and Kc using the network and compare it with experimental results. Table 5 gives the sample results of estimation for both the data sets. The average total error on training data and test data set is 5.65E-4 and 8.8E-2 for data set 1 and 2.1E-3 and 5.0E-2 for data set 2 respectively. It is clear from the error values and also from the sample results of estimation of Kac and Ka that the network has been able to estimate the values more accurately of the training data than the test data set. The test data contains data not used for training the network.

The results indicate that the estimation of values from the test data is acceptable for the purpose of evaluation. The MLP network has a good generalization capability and is able to estimate the values of Kac and Ka within about 90 % accuracy. One of the reasons for the less than satisfactory performance can be attributed to inadequate and less representative training samples [17]. It is thought that with more data representing all possible values, the performance will be improved.

However the MLP has some disadvantages i.e. it requires longer training time, has problems of local minima and has a fixed architecture, where the number of hidden neurons are fixed by trial and error (which consumes a significant amount of processing time). Hence, to overcome some of the limitations of MLP, a Radial Basis Function (RBF) based dynamic neural network algorithm namely Resource Allocation Network has been used for estimation of Kac and Ka.

3.3 RAN modelling results

RAN has been used to model the micro-abrasion-corrosion process for two pairs of materials as given above. The objective is to compare the performance of this network with the MLP in estimating the values of Kac and Ka. Several trials have been carried out to study the effect of various simulation parameters namely δ_{max} , κ and α, in order to generate a network architecture which is able to estimate Kac and Ka with minimum error. Table 6 gives the optimum simulation parameters for both data sets for desirable performance. Figures 5 and 6 show the growth pattern for RAN as it learns sequentially from the data for both data sets 1 and 2 respectively. In Figure 5, the addition of the hidden neurons takes place in different stages i.e. in the first 4 epochs 4 neurons are added, in the next 16 epochs, 5 neurons are added, from 21^{st} to 32^{nd} epoch, 9 neurons are added and there afterwards 20 neurons are added. Whereas in Figure 6, the network adds 16 hidden neurons in the first epoch itself and thereafter it remains constant for the remaining 5 epochs. It is clear that RAN adds hidden neurons almost equal to the number of patterns in the training set.

Table 7 gives the sample results of estimation for both the data sets. The average error for training data for both the data sets is almost negligible, meaning the network architecture is able to recognize all the data (100 % accuracy). For test data, the error is 0.13 for data set 1 and 0.48 for data set 2. It is clear from the error values and also from the sample results of estimation of Kac and Ka that the network has been able to estimate all the values in the training data, but the performance on the test data is unsatsfactory with errors as high as 0.48. One of the reasons for the less than satisfactory performance

on the test data set can be attributed to inadequate and less representative training samples [17]. With more representative data representing all possible values the performance should be improved.

3.4 Comparison of results of MLP and RAN

MLP is a widely used neural network architecture used in various applications, including tribology. MLP is widely used for modelling of processes. It offers a continuous approximation of a multivariable function, that is not analytically obtainable, but that is properly described by experimental data [20]. In this study MLP has been used for estimation of Kac and Ka and its performance has been compared with RAN, which is a relatively new neural network model used for estimation / modelling purposes.

RAN has poor generalization capability when compared to MLP because it memorizes the input data. MLP requires longer training time because it has the problem of local minima, since the learning process follows the gradient descent method. RAN has faster learning ability and produces small approximation errors when compared to MLP, but the hidden neurons added are more and is almost equal to the number of training patterns. This is the main limitation of RAN, as it generates a large network [17].

4.0 Conclusions

(i) In this paper an attempt has been made to use artificial neural networks (ANN) to model the micro-abrasion-corrosion processes of two tribological couples , a steel / polymer and ceramic / lasercarb coating in a carbonate/bicarbonate solution of pH 9.8.

(ii) MLP, which is used widely for prediction and classification, has been applied to model this process and estimate the values of Kac and Ka, two important parameters associated with the micro-abrasion-corrosion process.

(iii) The results have been evaluated using two classes of networks a Resource allocation Network (RAN), a Radial Base Function (RBF) network and a Multi-Layer Perceptron (MLP) network.

(iv) The less than satisfactory performance on test data of both MLP and RAN networks indicates that there are inadequate and less representative data samples. With more data samples, the performance of the networks can be definitely improved.

(v) The results clearly demonstrate that ANNs can be effectively used to model tribocorrosion processes. There is a need for conducting further experiments and data acquisition in order to model the process in a more effective manner.

References

1. D.Landolt., S.Mischler., M.Stemp., Electrochemical methods in tribocorrosion: a critical appraisal, Electrochim. Acta (2001) 46, 24–25.
2. S.C.Ferreira., E.Ariza., L.A.Rocha., J.R.Gomes., P.Carvalho., F.Vaz., A.C.Fernandes., L. Rebouta., E.Alves., Ph. Goudeau., J.P.Riviere., Tribocorrosion behaviour of ZrOxNy thin films for decorative applications, Surface and Coatings Technology (2005), 200, 6634-6639.
3. M.M. Stack., K. Chi., Mapping sliding wear of steels in aqueous condition, Wear (2003) 255, 456-465.

4. R.I.Trezona., D.N.Alsopp., I.M.Hutchings., Transitions between two-body and three-body abrasive wear: influence of test conditions in the microscale abrasive wear test, Wear (1999) 225-229, 205-214.
5. K.L.Rutherford., I.M.Hutchings., Theory and application of a microscale abrasive wear test, Journal Testing and Evaluation, JTEVA, (1997) 25, 2, 250-260.
6. M.M.Stack., M.T. Mathew., Mapping the microabrasion resistance of WC/Co based coatings in aqueous conditions, Surface and Coatings Technology, (2004) 183, 2-3, 337-346.
7. K.Adachi., I.M. Hutchings., Wear mode mapping for the microscale abrasion test, Wear (2003), 255, 23-29.
8. M.M.Stack., M.T.Mathew., Micro-abrasion transitions of metallic materials Wear (2003) 255, 14-22.
9. F.J.Buchanan., P.H. Shipway., Microabrasion-A simple method to assess surface degradation of UHMWPE following sterilization and ageing, Biomaterials, (2002), 23, 93-100.
10. A.J.Gant., M.G.Gee., A.T.May., Micro-abrasion of WC-Co hard metals in Corrosive media, Wear (2004) 256, 954-962.
11. M.M.Stack., M.T.Mathew., H.Jawan., On the construction of micro-abrasion maps for a steels/polymer couple in corrosive environment, Tribology International, (2005) 38, 9, 848-856.
12. J.L.Tipper., P.J.Firkins., A.A.Besong, P.S.M.Barbour., J.Nevelos.,M.H.Stone., E.Ingram, J.Fisher., Characterization of wear debris from UHMWPE on zirconia, metal-on-metal and alumina ceramic-on-ceramic hip prostheses generated in a physiological anatomical hip joint simulator, Wear (2001) 250, 1-12, 120-128
13. J.Ingram., J.B.Matthews., J.Pipper., M.Stone., J.Fisher., Comparison of the biological activity of grade GUR 1120 and GUR 415HP UHMWPE wear debris, Bio-Medical Materials Engineering, (2002) 12, 2, 177-188.
14. Mindora RIPA., Laurentiu FRANGU., A Survey of Artificial Neural Networks Applications in Wear and Manufacturing Processes, The Annals of University "DUNAREA DE JOS" of GALATI, FASCICLE VIII, ISSN 1221-4590, TRIBOLOGY, (2004) 35-42.
15. Z.Zhang., K.Friedrich., Artificial neural networks applied to polymer composites: a review, Composites Science and Technology, (2003) 63, 2029-2044.
16. P.Srinivasa Pai., Acoustic Emission Based Tool Wear Monitoring Using Some Improved Neural Network Methodologies, Ph. D Thesis, S.J.College of Engineering, University of Mysore, Mysore, (2004).
17. J.Platt., A resource allocating network for function interpolation, Neural Computation (1991) 3, 213-225.
18. L.Yingwei., N.Sundarajan., P.Saratchandran., Performance Evaluation of a Sequential Minimal RBF Neural Network Learning Algorithm, IEEE Trans. on Neural Networks, (1998) 9, 2, 308-318.
19. Z. Yue., P.Zhou., J.Shi., in Luedema K.C. Ed., Proc. Conf. Wear of Materials, ASME, New York, (1987), 763-768.
20. Laurentiu FRANGU., Minodora RIPA., Artificial Neural Networks Applications in Tribology – A Survey, NIMIA-SC 2001-2001 NATO Advanced Study Institute

on Neural Networks for Instrumentation, Measurement and Related Industrial Applications: Study Cases, Crema, Italy, 9-20 October 2001.

Captions of Tables

Table 1: Micro-abrasion-corrosion experimental details for polymer-steel couple.

Table 2: Micro-abrasion-corrosion experimental details for ceramic- Lasercarb coating couple.

Table 3: Weight change data for the micro-abrasion-corrosion interaction of mild polymer/steel couple at various potentials (a) –0.6 V (b) –0.4 V (c) –0.2 V (d) 0 V (e) +0.2 V.

Table 4: Weight change data for micro-abrasion-corrosion interaction of Ceramic-Ni-Cr/WC – Lasercarb coating, at fixed potential –0.2 V and various pHs. (a) pH 2
(b) pH 5.5 (c) pH 9.7 (d) pH 13.5

Table 5: Estimation of Kac and Ka by MLP (sample results)

Table 6: Simulation Parameters for RAN

Table 7: Estimation of Kac and Ka by RAN (sample results)

Captions of Figures

Figure 1: Schematic diagram of the experimental apparatus

Figure 2: Optical and SEM images (a) SiC- abrasive particles used in the experiments (b) Cross-sectional view of the Lasercarb coating, (c) Wear scar, Lasercarb coating, 5N, (d) Worn surface, Lasercarb coating, 5N, high magnification

Figure 3:MLP Neural Network architecture

Figure 4: RAN architecture

Figure 5:Growth pattern of RAN for data set 1

Figure 6:Growth pattern of RAN for data set 2

TABLES

Table 1 Micro-abrasion-corrosion experimental details for polymer-steel couple

Sample materials	mild steel
Ball materials	polypropylene
Speed	100rpm
Load	1- 5 N
Sliding Distance	3000rev or (235.50 m)
Slurry	Slurry composition: silicon carbide (4 μm diameter) with corrosive liquid ($0.5Na_2CO_3 + 0.5NaHCO_3$) (Concentration of 0.025g cm^{-3})

Table 2 Micro-abrasion-corrosion experimental details for ceramic-lasercarb -coating couple

Sample materials	Ni-Cr/WC Lasercarb coating (Composition: C-17.92%, Cr-9.33%, Ni-59.24%, W-7.39%, Si-4.76% Fe-1.35%, Thickness: 1189 μm, Hardness: 689 VHN)	
Ball materials	Ceramic (Si_3N_4)	
Speed	100rpm	
Load	1-5N	
Sliding distance	3000 rev or (235.50 m)	
Slurry	Slurry composition: silicon carbide (4 μm diameter) with corrosive liquid (Concentration of 0.025gcm^{-3}). The composition of the solutions are as follows	
	pH	**Composition of solution**
	2	Anhydrous sodium sulphate + sodium hydrogen sulphate monohydrate (0.5 M)
	5.5	Anhydrous sodium dihydrogen phosphate + anhydrous disodium hydrogen phosphate (0.5 M)
	9.7	Sodium bicarbonate + Sodium carbonate (0.5 M)
	13.5	Potassium hydroxide (0.5 M)

Table 3: Weight change data for the micro-abrasion-corrosion interaction of mild polymer/steel couple at various potentials (a) – 0.6 V (b) –0.4 V (c) –0.2 V (d) 0 V (e) +0.2 V.

(a) – 0.6 V						
Load (N)	Kac (g)	Kc (g)	Ka (g)	Kao (g) (weight loss at –0.96 V)	ΔKa (g)	Kc/Ka
1	1.40 E-04	1.03 E-04	3.70 E-05	1.3 E-04	-9.30 E-05	2.78
2	1.90 E-04	1.07 E-04	8.30 E-05	2.1 E-04	-1.27 E-04	1.29
3	2.30 E-04	1.03 E-04	1.27 E-04	2.7 E-04	-1.43 E-04	0.81
4	4.10 E-04	1.19 E-04	2.91 E-04	1.6 E-04	1.31 E-04	0.41
5	6.00 E-04	1.36 E-04	4.64 E-04	2.0 E-04	2.64 E-04	0.29

(b) – 0.4 V						
Load (N)	Kac (g)	Kc (g)	Ka (g)	Kao (g) (weight loss at –0.96 V)	ΔKa (g)	Kc/Ka
1	2.10 E-04	1.29 E-04	8.10 E-05	1.3 E-04	-4.90 E-05	1.59
2	3.30 E-04	1.50 E-04	1.80 E-04	2.1 E-04	-3.00 E-05	0.83
3	6.40 E-04	1.29 E-04	5.11 E-04	2.7 E-04	2.41 E-04	0.25
4	6.10 E-04	1.14 E-04	4.96 E-04	1.6 E-04	3.36 E-04	0.23
5	7.00 E-04	1.64 E-04	5.36 E-04	2.0 E-04	3.36 E-04	0.31

(c) – 0.2 V						
Load (N)	Kac (g)	Kc (g)	Ka (g)	Kao (g) (weight loss at –0.96 V)	ΔKa (g)	Kc/Ka
1	1.50 E-04	1.27 E-04	2.30 E-05	1.3 E-04	-1.07 E-04	5.52
2	2.00 E-04	1.22 E-04	7.80 E-05	2.1 E-04	-1.32 E-04	1.56
3	2.20 E-04	1.27 E-04	9.30 E-05	2.7 E-04	-1.77 E-04	1.37
4	2.60 E-04	1.34 E-04	1.26 E-04	1.6 E-04	-3.40 E-05	1.06
5	3.90 E-04	1.76 E-04	2.14 E-04	2.0 E-04	1.40 E-05	0.82

(d) 0 V						
Load (N)	Kac (g)	Kc (g)	Ka (g)	Kao (g) (weight loss at –0.96 V)	ΔKa (g)	Kc/Ka
1	1.30 E-04	1.23 E-04	7.00 E-06	1.3 E-04	-1.23 E-04	17.57
2	4.80 E-04	1.25 E-04	3.55 E-04	2.1 E-04	1.45 E-04	0.35
3	5.50 E-04	1.23 E-04	4.27 E-04	2.7 E-04	1.57 E-04	0.29
4	8.30 E-04	1.25 E-04	7.05 E-04	1.6 E-04	5.45 E-04	0.18
5	1.10 E-03	2.02 E-04	8.98 E-04	2.0 E-04	6.98 E-04	0.22

(e) + 0.2 V						
Load (N)	Kac (g)	Kc (g)	Ka (g)	Kao (g) (weight loss at –0.96 V)	ΔKa (g)	Kc/Ka
1	2.00 E-04	9.67 E-05	1.03 E-04	1.3 E-04	-2.67 E-05	0.94
2	2.30 E-04	8.64 E-05	1.44 E-04	2.1 E-04	-6.60 E-05	0.60
3	3.70 E-04	9.68 E-05	2.73 E-04	2.7 E-04	3.00 E-06	0.35
4	3.70 E-04	1.11 E-04	2.59 E-04	1.6 E-04	9.90 E-05	0.43
5	3.90 E-04	1.70 E-04	2.20 E-04	2.0 E-04	2.00 E-05	0.77

Table 4: Weight change data for micro-abrasion-corrosion interaction of Ceramic-Ni-Cr/WC – Lasercarb coating, at fixed potential –0.2 V and various pHs.

(a) pH 2						
Load (N)	Kac (g)	Kc (g)	Ka (g)	Kc/Ka	Kao (g) (Wear at – -1.0V)	ΔKa (g)
1	8.87 E-06	8.37 E-06	5.00 E-07	16.74	1.20 E-05	-1.15 E-05
2	1.32 E-05	7.84 E-06	5.36 E-06	1.46	1.30 E-05	-7.64 E-06
3	1.63 E-05	7.59 E-06	8.71 E-06	0.87	3.22 E-05	-2.34 E-05
4	1.02 E-05	7.04 E-06	3.16 E-06	2.23	3.32 E-05	-3.00 E-05
5	1.09 E-05	7.71 E-06	3.19 E-06	2.42	4.92 E-05	-4.60 E-05

(b) pH 5.5						
Load (N)	Kac (g)	Kc (g)	Ka (g)	Kc/Ka	Kao (g) (Wear at – -1.0V)	ΔKa (g)
1	1.32 E-05	7.91 E-06	5.29 E-06	1.50	5.36 E-06	-7.00 E-08
2	1.49 E-05	6.99 E-06	7.91 E-06	0.88	2.73 E-05	-1.94 E-05
3	1.01 E-05	6.34 E-06	3.76 E-06	1.69	3.11 E-05	-2.73 E-05
4	1.48 E-05	6.08 E-06	8.72 E-06	0.70	1.14 E-05	-2.68 E-06
5	1.89 E-05	6.17 E-06	1.27 E-05	0.48	2.47 E-05	-1.20 E-05

(c) pH 9.7						
Load (N)	Kac (g)	Kc (g)	Ka (g)	Kc/Ka	Kao (g) (Wear at – -1.0V)	ΔKa (g)

1	3.84 E-05	8.24 E-06	3.02 E-05	0.27	3.22 E-05	-2.04 E-06
2	3.72 E-05	7.95 E-06	2.93 E-05	0.27	3.36 E-05	-4.35 E-06
3	4.04 E-05	8.22 E-06	3.22 E-05	0.26	3.19 E-05	2.80 E-07
4	3.13 E-05	8.84 E-06	2.25 E-05	0.39	2.88 E-05	-6.34 E-06
5	4.16 E-05	8.44 E-06	3.32 E-05	0.25	3.19 E-05	1.26 E-06

(d) pH 13.5						
Load (N)	Kac (g)	Kc (g)	Ka (g)	Kc/Ka	Kao (g) (Wear at – -1.0V)	ΔKa (g)
1	9.73 E-06	8.09 E-06	1.64 E-06	4.93	2.35 E-05	-2.19 E-05
2	1.03 E-05	8.32 E-06	1.98 E-06	4.20	2.29 E-05	-2.09 E-05
3	1.08 E-05	7.90 E-06	2.90 E-06	2.72	2.36 E-05	-2.07 E-05
4	1.25 E-05	7.17 E-06	5.33 E-06	1.35	1.04 E-05	-5.07 E-06
5	1.29 E-05	8.02 E-06	4.88 E-06	1.64	2.51 E-05	-2.02 E-05

Table 5 Estimation of Kac and Ka by MLP (sample results)

(a) Data set 1					
Sl.No.	Kac (expt.)	Ka (expt.)	Kac (network)	Ka (network)	Total error
Training data					
1	0.3170	0.7870	0.3026	0.7881	1.05 E-05
2	1.0000	1.0000	0.9703	0.9558	1.419 E-03
3	0.8710	0.6950	0.9205	0.6739	1.446 E-03
4	0.5130	0.6930	0.5213	0.6892	4.1265 E-05
5	0.5130	0.5690	0.5127	0.5657	5.3693 E-06
Test data					
1	0.2330	0.7570	0.0213	0.5244	0.0495
2	0.4710	0.9150	0.8718	0.8617	0.0817
3	0.5640	0.7220	0.2515	0.3941	0.1026
4	1.0000	0.6190	0.4362	0.8646	0.1891
5	1.0000	1.0000	0.9999	0.8235	0.0156

(b) Data set 2					
Sl.No.	Kac (expt.)	Ka (expt.)	Kac (network)	Ka (network)	Total error
Training					

data					
1	0.8100	0.9370	0.8188	0.9043	5.73 E-04
2	0.6690	0.9210	0.6673	0.8921	4.2 E-04
3	0.7830	0.7690	0.7883	0.7564	9.3610 E-05
4	0.8940	0.8990	0.8881	0.9649	2.188 E-03
5	1.0000	0.9640	0.9427	0.9639	1.642 E-03
Test data					
1	0.5440	1.0000	0.0533	0.8892	0.1265
2	0.9710	0.9300	0.6402	0.9316	0.0547
3	0.7880	0.8840	0.9144	0.9618	0.0110
4	0.9690	0.8620	0.9147	0.9653	6.805 E-03

Table 6 Simulation Parameters for RAN

Data set 1		**Data set 2**	
e_{min}	0.00005	e_{min}	0.00005
δ_{max}	0.5	δ_{max}	0.5
δ_{min}	0.01	δ_{min}	0.1
κ	0.2	κ	0.5
τ	700	τ	100
α	0.1	α	0.5
No. of Epochs	62	No. of Epochs	6
No. of RBF units (hidden neurons)	20	No. of RBF units (hidden neurons)	16

Table 7 Estimation of Kac and Ka by RAN (sample results)

(a) Data set 1					
Sl.No.	Kac (expt.)	Ka (expt.)	Kac (network)	Ka (network)	Total error
Training data					
1	0.3170	0.7870	0.3163	0.7883	2.2302 E-6
2	1.0000	1.0000	1.0016	1.0019	6.2780 E-6

3	0.8710	0.6950	0.8717	0.6962	1.8727 E-6
4	0.5130	0.6930	0.5136	0.6934	4.3803 E-7
5	0.5130	0.5690	0.5133	0.5690	6.8232 E-8
Test data					
1	0.2330	0.7570	0.6544	0.6947	0.1815
2	0.4710	0.9150	0.6545	0.6947	0.0822
3	0.5640	0.7220	0.6608	0.6929	0.0102
4	1.0000	0.6190	0.6279	0.7119	0.1471
5	1.0000	1.0000	0.6279	0.7119	0.2213

(b) Data set 2					
Sl.No.	Kac (expt.)	Ka (expt.)	Kac (network)	Ka (network)	Total error
Training data					
1	0.8100	0.9370	0.8092	0.9359	1.7189 E-6
2	0.6690	0.9210	0.6696	0.9225	2.5037 E-6
3	0.7830	0.7690	0.7841	0.7718	9.1722 E-6
4	0.8940	0.8990	0.8949	0.9005	3.1113 E-5
5	1.0000	0.9640	0.9999	0.964	3.5527 E-13
Test data					
1	0.5440	1.0000	0.0063	0.0129	1.2634
2	0.9710	0.9300	0.6290	0.9173	0.1172
3	0.7880	0.8840	0.5989	0.6939	0.0719
4	0.9690	0.8620	0.4327	0.4367	0.4685

FIGURES

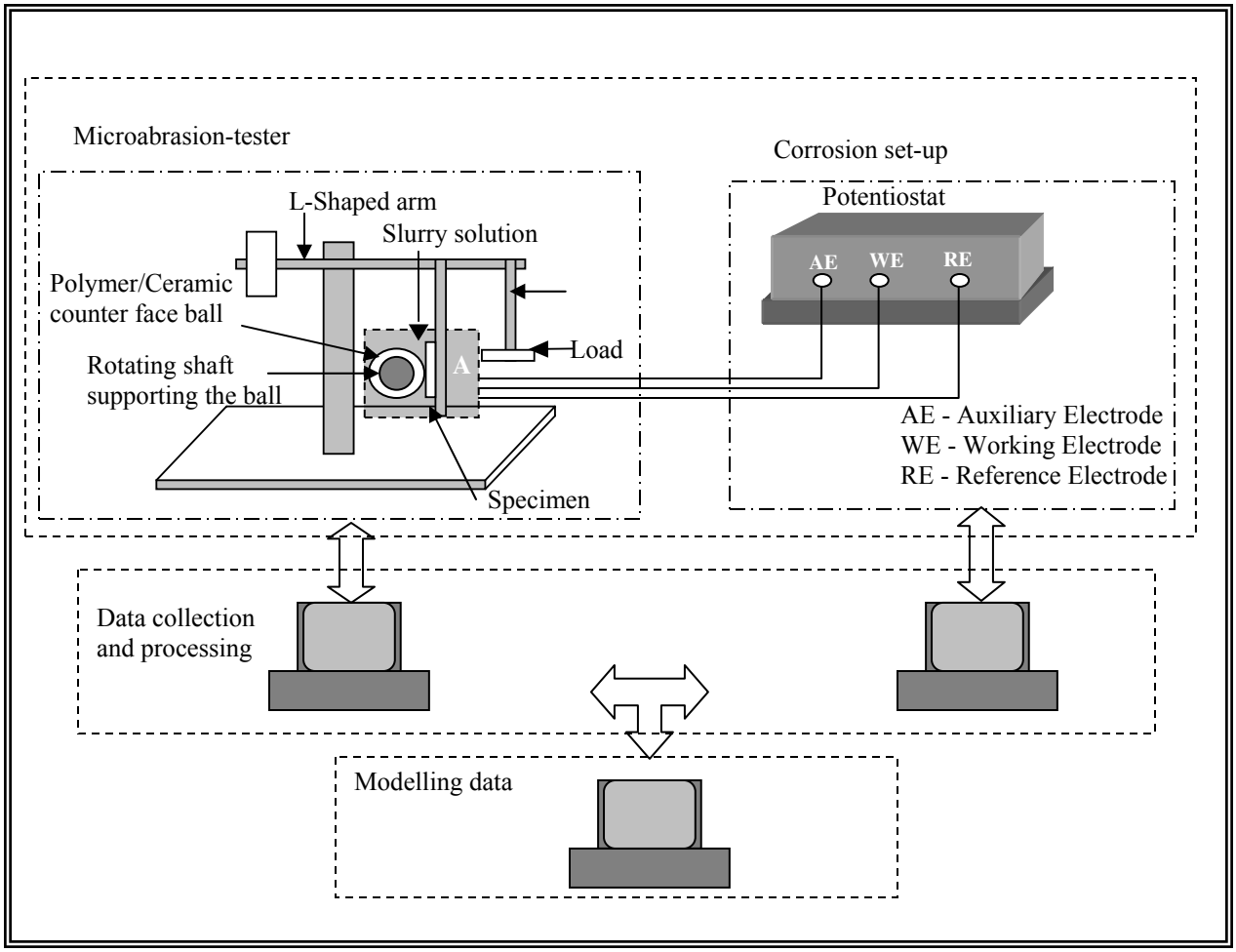

Figure 1. Schematic diagram of experimental apparatus

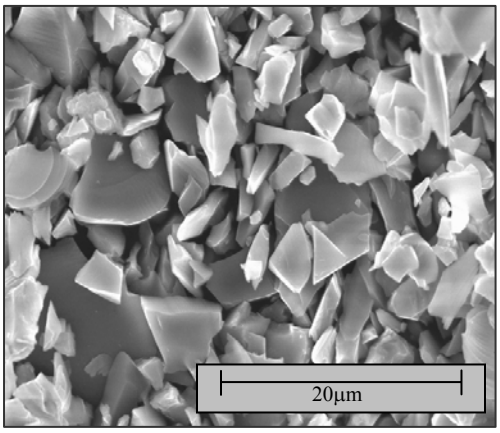

(a) SiC- abrasive particles used in the experiments

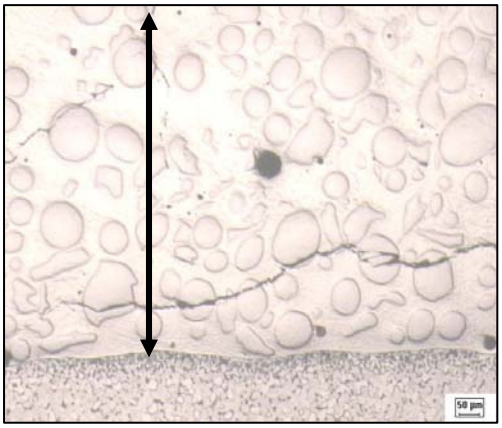

(b) Cross-sectional view of the Lasercarb coating

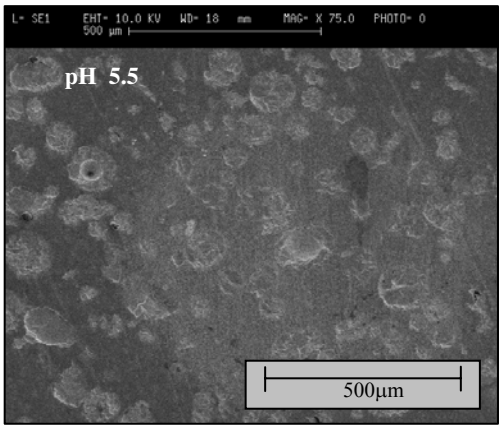

(c) Wear scar, Lasercarb coatings, 5N.

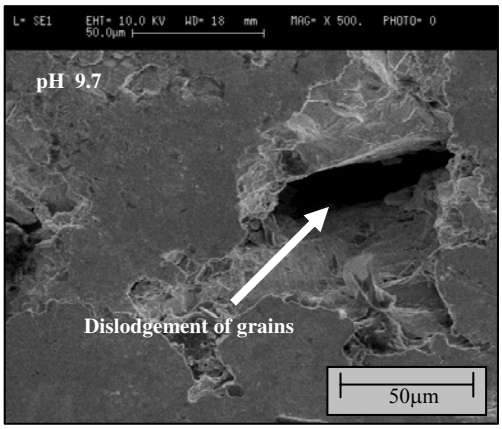

(d) Worn surface, Lasercarb coating, 5N, high magnification

Figure 2. Optical micrograph and SEM images

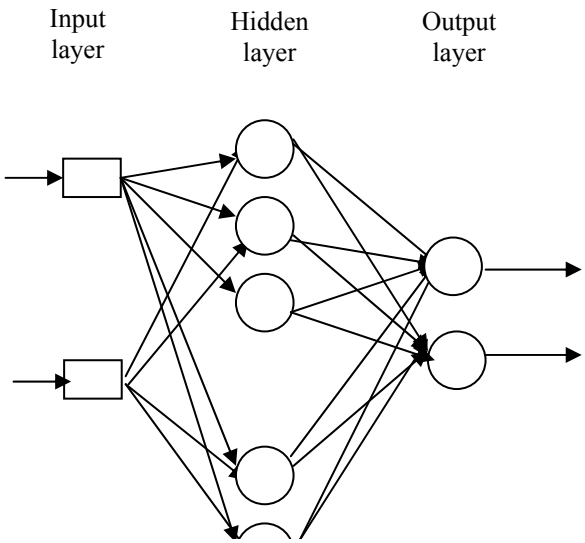

Figure 3. MLP Neural Network architecture

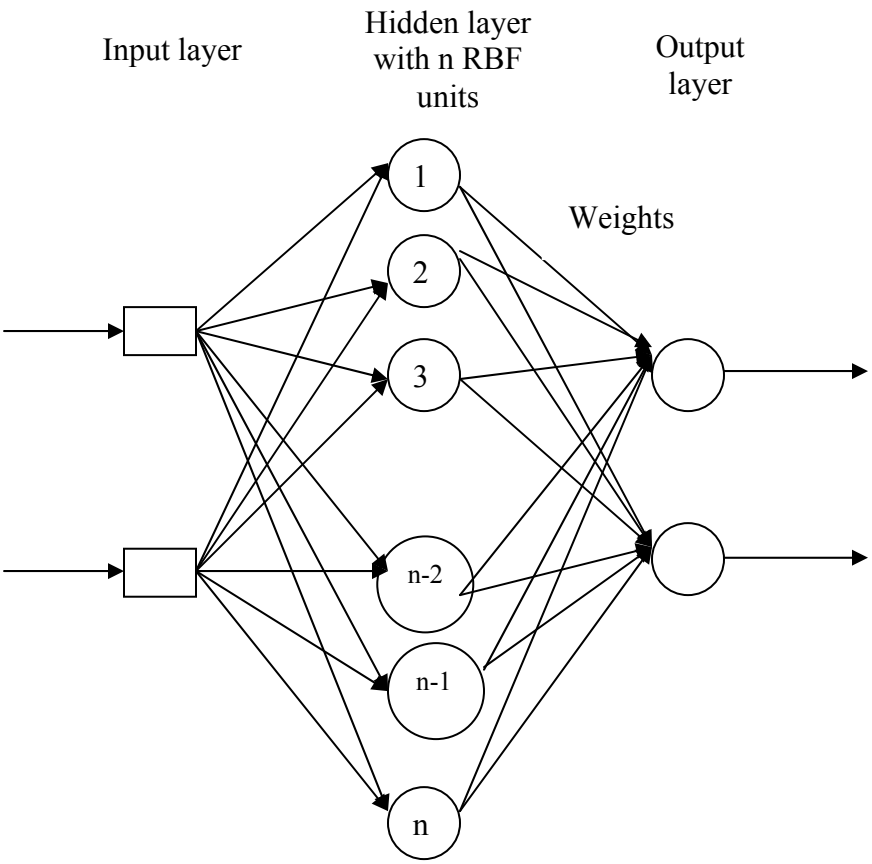

Figure 4. RAN architecture

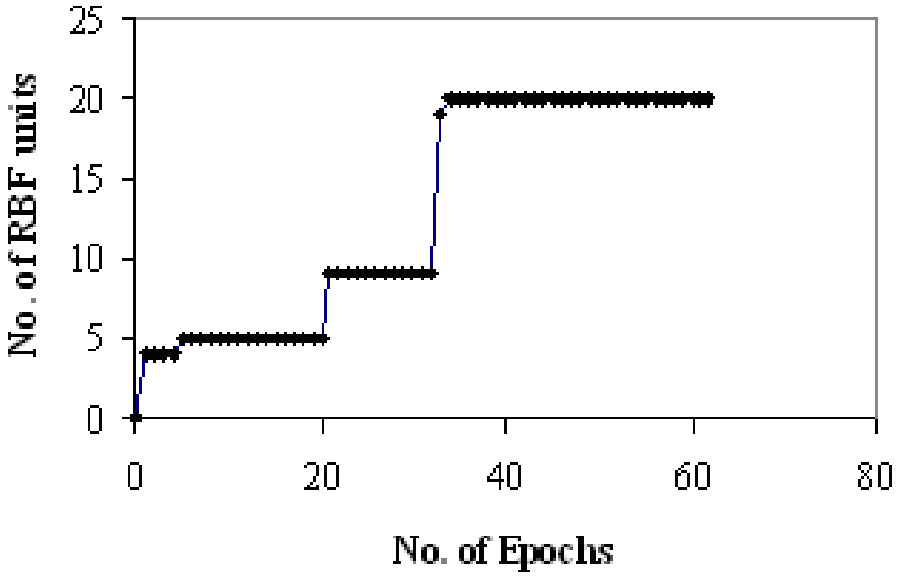

Figure 5. Growth pattern of RAN for Data set 1

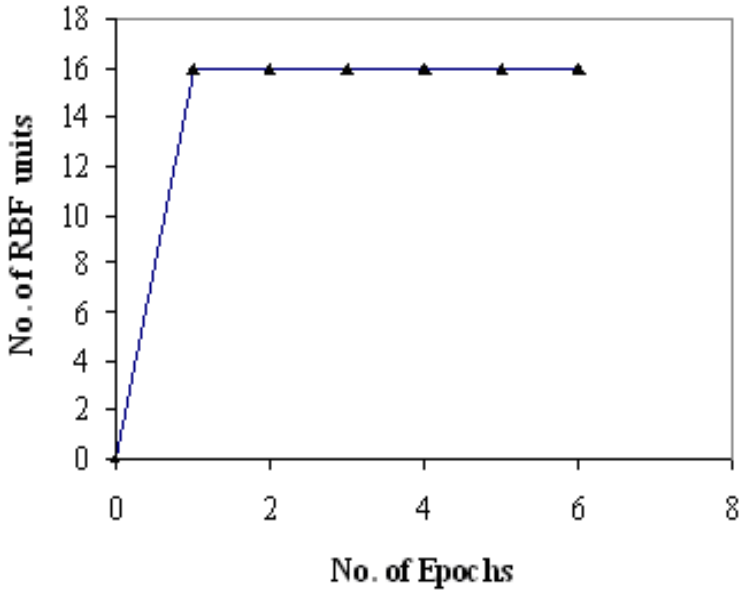

Figure 6. Growth pattern of RAN for Data set 2